Atmospheric pressure chemical vapor deposition of amorphous tungsten doped vanadium dioxide for smart window applications

Dimitrios Louloudakis[1,2*], **Dimitra Vernardou**[1], **Emmanuel Spanakis**[3], **Mirela Suchea**[4], **George Kenanakis**[5], **Martyn Pemble**[6], **Constantine Savvakis**[1,7], **Nikolaos Katsarakis**[1,4,5], **Emmanuel Koudoumas**[1,4] **and George Kiriakidis**[2,5]

[1]*Center of Materials Technology & Photonics, School of Applied Technology, Technological Educational Institute of Crete, 710 04 Heraklion, Crete, Greece*

[2]*Department of Physics, University of Crete 711 00 Heraklion, Crete, Greece*

[3]*Department of Materials Science & Technology, University of Crete 711 00 Heraklion, Crete, Greece*

[4]*Department of Electrical Engineering, School of Applied Technology, Technological Educational Institute of Crete, 710 04 Heraklion, Crete, Greece*

[5]*Institute of Electronic Structure & Laser, Foundation for Research & Technology- Hellas, P.O. Box 1527, Vassilika Vouton, 711 10 Heraklion, Crete, Greece*

[6]*Tyndall National Institute, University College Cork, Lee Maltings, Prospect Row, Cork, Ireland*

[7]*Mechanical Engineering Department, School of Applied Technology, Technological Educational Institute of Crete, 710 04 Heraklion, Crete, Greece*

[*]Corresponding author. E-mail: dimitr17@yahoo.gr

ABSTRACT

Amorphous tungsten doped vanadium dioxide coatings were grown on SnO_2-precoated glass substrates using the atmospheric pressure chemical vapor deposition of vanadium (V) triisopropoxide and tungsten (VI) isopropoxide at 450 ^{o}C without an oxygen source. The effect of N_2 flow rate through the tungsten's precursor bubbler was examined keeping the respective flow rate through the vanadium's precursor bubbler at 4 L min^{-1} for a growth period of 30 min. They were characterized by x-ray diffraction, Raman and x-ray photoelectron spectroscopy, field-emission scanning electron microscopy and UV-vis/IR transmittance. The samples grown using 0.4 L min^{-1} N_2 flow rate through the tungsten precursor's bubbler, showed the greatest reduction in transition temperature from 65.5 in granular VO_2 to 44 ^{o}C in worm-like $V_{0.985}W_{0.015}O_2$ structures approaching that required for commercial use as a smart window coating. Copyright © 2016 VBRI Press.

Keywords: APCVD; tungsten doped vanadium dioxide; thermochromic material.

Introduction

In recent years, vanadium oxides have attracted a lot of interest due to their fascinating features. As an example, vanadium pentoxide (V_2O_5) presents cation intercalation characteristics [1] and can be used in technological applications such as Li-ion batteries [2], electrochromic devices [3] etc. Attention has also been given to vanadium dioxide (VO_2), which presents a monoclinic structure below transition temperature (T_c) exhibiting a semiconducting behavior, while above T_c, it accompanies a phase transition to rutile with metallic characteristics [4]. This transition results in a change in optical transmittance and reflectivity in regions of the spectrum that are major contributors to solar heating. As such, VO_2 has potential application in the area of thermochromic smart windows [5]. However, its T_c is of the order of 68 ^{o}C, which needs to be reduced to find practical use as a window coating.

Doping metal ions such as tungsten into the VO_2 lattice is an effective way to lower the T_c to about 25 ^{o}C for 2 at.% loading [6, 7]. The tungsten doped VO_2 coatings have been prepared by rf. Sputtering [8], sol-gel [9], hydrothermal method [10] and chemical vapor deposition (CVD) [11-14]. Among these techniques, CVD, when performed at atmospheric pressure without an oxygen source (but only with the vanadium and tungsten

precursors), would make such a process compatible with high volume, in-line glass manufacturing processes because the production process is simplified and the cost is decreased. As a result, various precursors have been used such as vanadium (IV) chloride [**12**] and vanadyl (IV) acetylacetonate [**13**] for vanadium precursor, tungsten (VI) ethoxide [**12**] and tungsten chloride [**14**] for tungsten precursor along with O_2 cylinder and water in an additional bubbler.

Based on our previous work [**15**], the deposition of tungsten doped VO_2 was accomplished using the atmospheric pressure CVD (APCVD) reaction of vanadium (V) triisopropoxide oxide ($VO(OC_3H7)_3$) and tungsten isopropoxide oxide ($W(OC_3H_7)_6$) precursors. In this case, the coatings growth took place without an oxygen source in contrast with others reported which reduces the production cost and makes the system more attractive for large scale manufacturing processes. The effect of N_2 flow rate though the tungsten precursor's bubbler on the value of T_c and the coatings properties was studied.

Experimental

The tungsten doped vanadium dioxide coatings were deposited using a homemade APCVD as reported previously [**16-18**]. $VO(OC_3H_7)_3$ (96%, Alfa Aesar) and $W(OC_3H_7)_6$ (5% w/v in isopropanol, Alfa Aesar) were placed into separate bubblers at 50 ^{o}C and room temperature, respectively. All depositions were carried out at 450 ^{o}C for 30 min. High purity N_2 (99.995 %) was used as the system gas in all CVD reactions. The N_2 gas flow rate through the vanadium precursor bubbler was remained constant at 4.0 L min^{-1}, while it was varied from 0.2 to 1.0 L min^{-1} through the tungsten precursor's bubbler. In all cases, the total gas flow rate was 12 L min^{-1}. The substrate was SnO_2-precoated glass (Uniglass, Greece) of 2.5 cm x 2.5 cm x 0.4 cm. Prior to deposition, all substrates were cleaned into propan-2-ol for 10 min, then acetone for 10 min using an ultrasonic bath, and they were finally rinsed with distilled water and dried with N_2 gas.

X-ray diffraction (XRD) measurements were carried out in a Siemens D5000 Diffractometer for $2\theta = 10.00$-60.00, step size 0.02 ^{o} and step time 60 s/^{o} with glancing theta angle equal with 2, 3 and 5 degrees. Raman spectroscopy was done in a Nicolet Almega XR micro-Raman system using a 514 nm laser line at an incident intensity of 10 mW μm^{-2}. X-ray photoelectron spectroscopy (XPS) measurements were carried out in a XSAM800 Instrument using un-monochromated Mg K_α radiation as X-ray source with line width of 0.8 eV and pass energy of 20 eV. An Argon-sputtering gun was used to clean the surfaces of carbon for 150 s at 3 keV. The binding energy (E_B) values were referenced to C1s peak at 258 eV. Surface characterization was accomplished in a Jeol JSM-7000F field-emission electron microscope (FE-SEM). The magnification is X50000 and the bar is equal with 100 nm. Samples were over-coated with a thin film of gold prior to analysis to prevent charging. The transmittance measurements were performed in a Perkin Elmer Lambda 950 spectrophotometer over the wavelength range of 250-2500 nm at 25 and 90 ^{o}C as already reported previously [**15**]. Finally, transmittance-temperature studies were done at 1500 ± 20 nm between 25 and 90 ^{o}C.

Results and discussion

The coatings produced during the APCVD reaction of VO $(OC_3H_7)_3$ and W $(OC_3H_7)_6$ were green, adhesive and passed the Scotch tape test [**19**]. They were insoluble in water and acetone. Furthermore, all samples presented similar properties (structural, morphological, thermochromic performance) after storage for six months indicating long term stability at environmental conditions. Finally, the coating growth showed good reproducibility (experiments were performed three times each).

A proposed mechanism of VO_2 growth has been given in our previous work [**15**] and we assume a similar chemical reaction for tungsten doped VO_2. The presence of tungsten into the lattice of VO_2 creates defects and as a result there is a shift in the transition temperature [**12**].
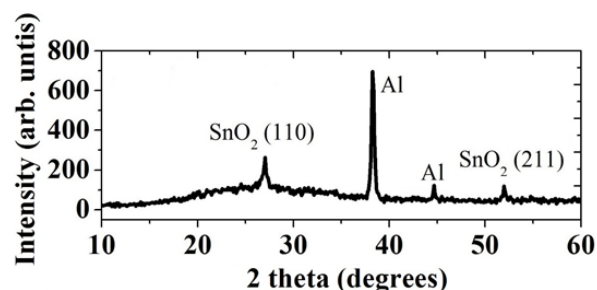
Fig. 1. XRD patterns of the as-grown tungsten doped VO_2 coating using 0.4 L min^{-1} N_2 flow rate through the tungsten precursor's bubbler. All peaks correspond to the substrate and Al holder, indicating that the coating is amorphous.

Structure

XRD pattern of the as-deposited tungsten doped VO_2 coating using 0.4 L min^{-1} N_2 flow rate through the tungsten precursor's bubbler (**Fig. 1**) presents peaks related with the underlying substrate (two peaks at 26.5^o and 51.5^o with Miller indices (110) and (211) respectively) and the Al holder (two peaks at 38.3^o and 44.6^o). All coatings show similar behavior indicating that they are largely amorphous.

Fig. 2 (**a, b**) indicate the Raman spectra of the coatings grown for 0 and 0.4 L min^{-1} N_2 flow rate through the tungsten precursor's bubbler, respectively.
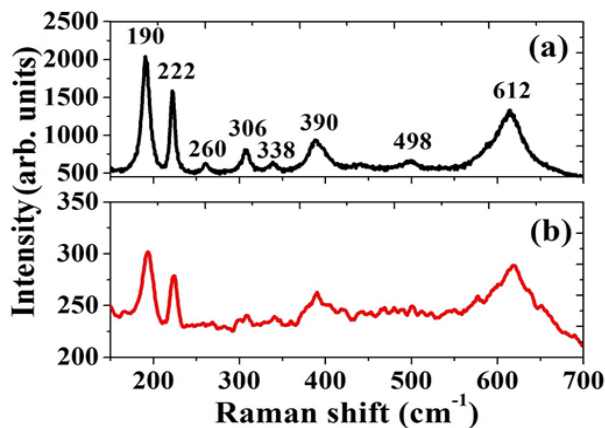
Fig. 2. Raman spectra of pure VO_2 (a) and tungsten doped VO_2 (b) grown on SnO_2-precoated glass substrate for 30 min by APCVD at 450 ^{o}C using 0 and 0.4 L min^{-1} nitrogen gas flow rate through the tungsten precursor's bubbler, respectively.

Fig. 2 (**a**) shows features at 190, 222, 260, 306, 338, 390, 498 and 612 cm^{-1} due to the monoclinic VO$_2$ phase [**18, 20**]. All Raman bands are attributed to an A$_g$ symmetry mode. Finally, the Raman band at 614 cm^{-1} is likely to result from stretching modes of the V–O–V bridging bonds, while the other Raman bands are assigned to bending motions of the vanadium–oxygen bonds [**18, 20**]. Regarding the tungsten doped VO$_2$, broadening of the Raman bands with a significant reduction of their intensity (**Fig. 2 (b)**) is indicated in comparison with the undoped VO$_2$ due to the presence of defects caused by the dopant ions in the lattice [**12**].
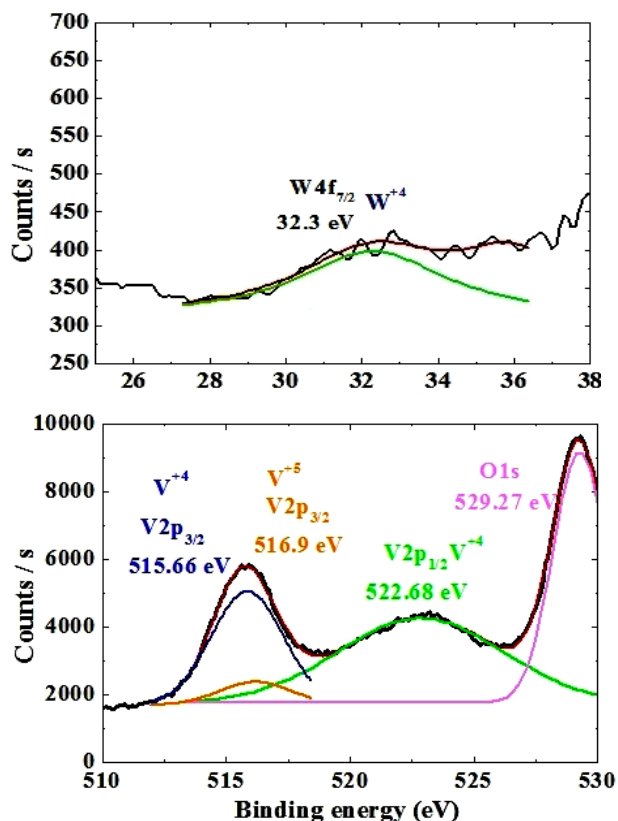
Fig. 3. XPS analysis for the tungsten doped VO$_2$ coating grown using 0.4 L min^{-1} N$_2$ flow rate through the tungsten bubbler. The left figure shows the W4f region of the sample and the right the V2p region of the sample.

XPS analysis was used to elucidate the oxidation states of the ions present for the coating grown using 0.4 L min^{-1} N$_2$ flow rate through the tungsten precursor's bubbler as shown in **Fig. 3**. It indicates that vanadium is present as V^{+4} with V3p$_{3/2}$, V3p$_{1/2}$ at binding energies of 515.16 eV and 522.68 eV respectively and V^{+5} at binding energy of 516.9. The reason of the existence of a mixture of different valence states of vanadium is that the detection depth of the XPS is only a few nanometers, in which the +4 valence of vanadium is easily oxidized to +5 valences [**21**]. Tungsten 4f peak is assigned as W^{+4} with W4f$_{7/2}$ at binding energy of 32.3 eV indicating the tungsten doping into VO$_2$ [**12, 22**]. Based on the XPS spectra, tungsten isopropoxide oxide is found to be able to dope VO$_2$ with 1.5 at. %. Finally, carbon contamination from the alkoxide precursors is observed in all samples making difficult the tungsten's detection.
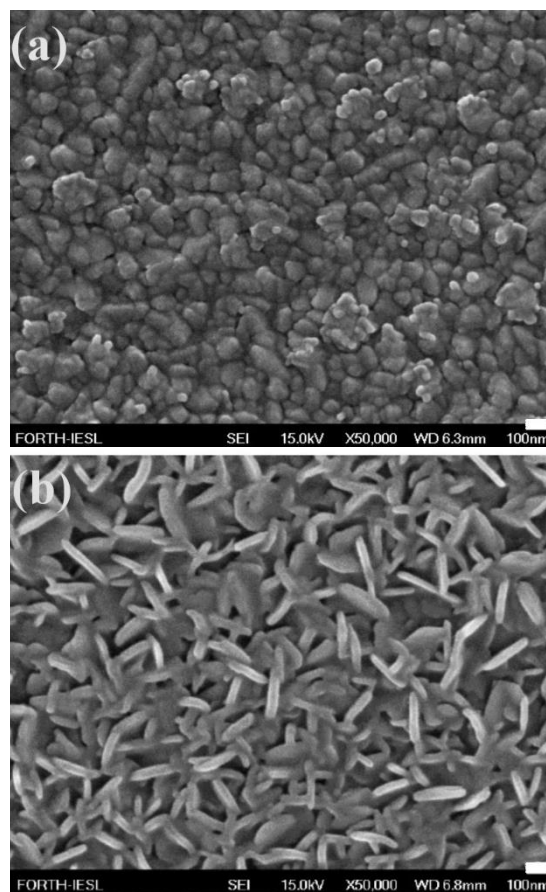
Fig. 4. FE-SEM images of the as-prepared pure VO$_2$ (a) and tungsten doped VO$_2$ (b) coatings, using 0 and 0.4 L min^{-1} N$_2$ gas flow rate through the tungsten precursor's bubbler, respectively.

Morphology

FE-SEM images of the coatings grown for 0 and 0.4 L min^{-1} N$_2$ flow rate through the tungsten precursor's bubbler are shown in **Fig. 4** (**a, b**). From these Figures, it is seen that the surface features change from granular [**15**] to worm-like structures indicating the strong effect of tungsten doping on morphology. It has also been reported previously that the doping in VO$_2$ changes the morphology [**11-13**, **23**] without explaining possible mechanism. For N$_2$ flow rate less and larger than 0.4 L min^{-1}, the morphology remains unchanged showing that there is either less than 1.5 at. % or no tungsten doped in VO$_2$.

Thermochromic behavior

Fig. 5 (**a**) displays the transmittance curves as a function with wavelength at 25 and 90 ^{o}C for the SnO$_2$-precoated glass substrate (inset) and the as-grown tungsten doped VO$_2$ coating using 0.4 L min^{-1} N$_2$ flow rate through the tungsten precursor's bubbler. Despite the fact that the tungsten doped VO$_2$ sample is amorphous, it displays a decrease in IR transmittance and little change in the visible region as required for smart window coating applications. This behavior is in agreement with the literature indicating that the thermochromic performance of the samples can be further enhanced as they approach the crystalline monoclinic phase [**15, 24-27**]. On the other hand, the glass substrate does not present change in transmittance upon

heating indicating that the respective reduction observed previously is solely due to the doped sample.
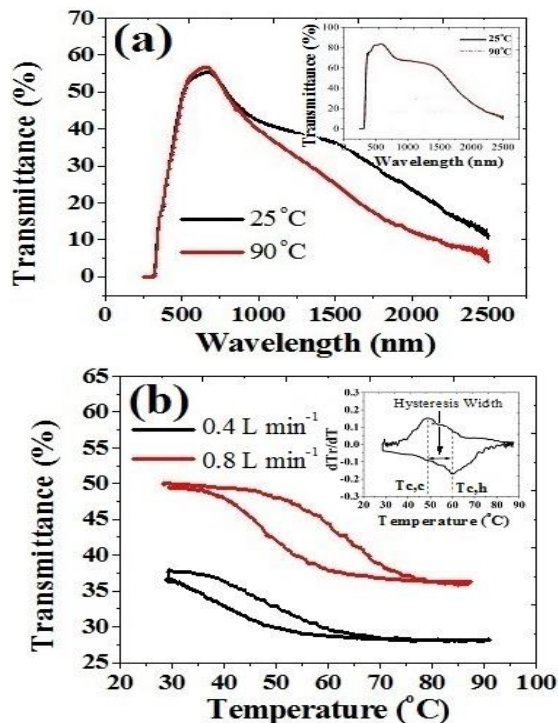
Fig. 5. (a) Transmittance spectra at 25 and 90 °C of the tungsten doped VO_2 coatings grown using 0.4 L min^{-1} N_2 flow rate through the tungsten precursor's bubbler. Inset in (a) presents the transmittance spectra of the substrate at 25 and 90 °C. (b) Transmittance-temperature studies at 1500 nm of the 0.4 (black line) and 0.8 L min^{-1} (red line) N_2 flow rate through the tungsten precursor's bubbler. Inset in (b) presents the schematic presentation of the transmittance differential dTr/dT vs. Temperature for the tungsten doped VO_2 coating grown for 0.8 L min^{-1} N_2 flow rate through the tungsten precursor's bubbler at 450 °C.

The thermochromic parameters including T_c, hysteresis width (HW) and change in transmittance (ΔT) at 1500 nm are estimated by the curve of transmittance as a function with temperature as shown in **Fig. 5b** for 0.4 and 0.8 L min^{-1} N_2 flow rate through the tungsten precursor's bubbler (the curve for 0 L min^{-1} has been reported elsewhere[15]). From this information, a plot of d(Transmittance)/d(Temperature)–Temperature is obtained (see **Fig. 5** (**b**) inset**)** [15, 28] and the thermochromic parameters are estimated for all samples (**Table 1**).

Table 1. The thermochromic parameters including T_c, HW and ΔT of the as-grown coatings using 0.0, 0.4, 0.6 and 0.8 L min^{-1} N_2 flow rate through the tungsten precursor's bubbler.

N_2 flow rate through the tungsten precursor's bubbler / L min^{-1}	0.0	0.4	0.6	0.8
/ °C	65.5	44	52	55
HW / °C	19	7	10	12
ΔT / %	20	9	10	13

From **Table 1**, it is indicated that the as-grown coating using 0.4 L min^{-1} N_2 flow rate through the tungsten precursor's bubbler presents the largest T_c drop by 21.5 °C compared with the undoped one [15] indicating the doping

of tungsten. In addition, the difference in transmittance at 1500 nm and the hysteresis width of the same sample are in agreement with other techniques for 1.5 at. % tungsten doped VO_2 such as sol-gel [29], sputtering [30] and APCVD using vanadium chloride [13]. Finally, the thermochromic behavior presents stability with time as shown from the similarity of the transmittance curves as a function with temperature after six months storage in air (**Fig. 6**).

The capability to decrease T_c via control of the N_2 flow rate through the tungsten precursor's bubbler without the use of an oxidant source by APCVD, has been demonstrated in this work. Improvements to the system could however be made to grow coatings with larger tungsten loadings.
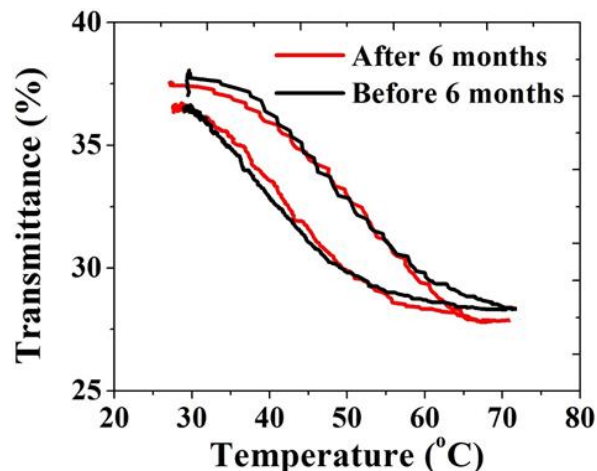
Fig. 6. The hysteretic behavior of the as-grown tungsten doped VO_2 coating for 0.4 L min^{-1} N_2 flow rate through the tungsten precursor's bubbler before (black line) and after 6 months (red line).

Conclusion

Amorphous tungsten doped VO_2 was deposited on SnO_2-precoated glass using an APCVD without an oxygen source. The $W(OC_3H_7)_6$ was found to be able to dope VO_2 with tungsten 1.5 at. % lowering the T_c to 44 °C from 65.5 °C using an optimum N_2 flow rate of 0.4 L min^{-1} through the tungsten precursor's bubbler. The presence of tungsten in the lattice of VO_2 changed the surface morphology to worm-like from granular structure. A benefit of the particular system is that oxygen source is not required simplifying the operations by the removal of bubbler and other vapor systems.

Reference
1. Wang, Y.; Cao, G.; Electrochim. Acta. 2006, 51, 4865.
   DOI:10.1016/j.electacta.2006.01.026
2. Seng, K. H.; Liu, J.; Guao, Z. P.; Chen, Z. X.; Jia, D.; Liu, H. K.; Electrochem. Commun. 2011, 13, 383.
   DOI: 10.1016/j.elecom.2010.12.002

3. Talledo, A.; Andersson, A. M.; Granqvist, C. G.; J. Mat. Res. 1990, 506, 1253.
DOI: 10.1557/JMR.1990.1253

4. Goodenough, J. B.; J. Solid State Chem. 1971, 3, 490.
DOI: 10.1016/0022-4596(71)90091-0

5. Babulanam, S. M.; Eriksson, T. S.; Niklasson, G. A.; Granqvist, C. G.; Sol. Energ. Mater. 1987, 16, 347.
DOI:10.1016/0165-1633(87)90029-3

6. Burkhardt, W.; Christmann, T.; Meyer, B. K.; Niessner, W.; Schalch, D.; Scharmann, A.; Thin Solid Films 1999, 345, 229.
DOI:10.1016/S0040-6090(98)01406-0

7. Blackman, C. S.; Piccirillo, C.; Binions, R.; Parkin, I. P.; Thin Solid Films 2009, 517, 4565.
DOI:10.1016/j.tsf.2008.12.050

8. Sobhan, M. A.; Kivaisi, R. T.; Stjerna, B.; Granqvist, C. G.; Sol. Energ. Mat. Sol. C. 1996, 44, 451.
DOI:10.1016/S0927-0248(95)00051-8

9. Cho, J. -H.; Byun, Y. -J.; Kim, J. -H.; Lee, Y. -J.; Jeong, Y. -H.; Chun, M. -P.; Paik, J. -H.; Sung, T. H.; Ceram. Int. 2012, 1, S589.
DOI:10.1016/j.ceramint.2011.05.104

10. Shi, J.; Zhou, S.; You, B.; Wu, L.; Sol. Energ. Mat. Sol. C. 2007, 19, 1856
DOI:10.1016/j.solmat.2007.06.016

11. Manning, T. D.; Parkin, I. P.; J. Mater. Chem. 2004, 14, 2554.
DOI: 10.1039/B403576N

12. Manning, T. D.; Parkin, I. P.; Pemble, M. E.; Sheel, D.; Vernardou, D.; Chem. Mater. 2004, 16, 744.
DOI: 10.1021/cm034905y

13. Binions, R.; Piccirilo, C.; Parkin, I. P.; Surf. Coat. Tech. 2007, 201, 9369.
DOI:10.1016/j.surfcoat.2007.03.026

14. Blackman, C. S.; Piccirillo, C.; Binions, R.; Parkin, I. P.; Thin Solid Films 2009, 517, 4565.
DOI:10.1016/j.tsf.2008.12.050

15. Vernardou, D.; Louloudakis, D.; Spanakis, E.; Katsarakis, N.; Koudoumas, E.; Sol. Energ. Mat. Sol. C. 2014, 128, 36.
DOI:10.1016/j.solmat.2014.04.033

16. Vernardou, D.; Pemble, M. E.; Sheel, D. W.; Chem. Vapor Depos. 2006, 12, 263.
DOI: 10.1002/chin.200631017

17. Louloudakis, D.; Vernardou, D.; Spanakis, E.; Katsarakis, N.; Koudoumas, E.; Physics Procedia 2013, 46, 137.
DOI:10.1016/j.phpro.2013.07.055

18. Vernardou, D.; Paterakis, P.; Drosos, H.; Spanakis, E.; Povey, I. M.; Pemble, M. E.; Koudoumas, E.; Katsarakis, N.; Sol. Energ. Mat. Sol. C. 2011, 95, 2842.
DOI:10.1016/j.solmat.2011.05.046

19. Manning, T. D.; Parkin, I. P.; Clark, R. J. H.; Sheel, D.; Pemble, M. E.; Vernardou, D.; J. Mater. Chem. 2002, 12, 2936.
DOI: 10.1039/B205427M

20. Vernardou, D.; Pemble, M. E.; Sheel, D. W.; Surf. Coat. Tech. 2004, 188-189 250.
DOI:10.1016/j.surfcoat.2004.08.037

21. Shi, Q.W.; Huang, W.X.; Xu, Y.J.; Zhang, Y.X.; Yue, F.; Quiao, S.; Zheng, S.P.; Yan, J.Z.; J. Phys. D: Appl. Phys. 2012, 45, 385302
DOI:10.1088/0022-3727/45/38/385302

22. Huang, Z.; Chen, C.; Lv, C.; Chen, S.; J. Alloys Compd. 2013, 564, 158.
DOI:10.1016/j.jallcom.2013.02.108

23. Song, L.; Zhang, Y.; Huang, W.; Shi, Q.; Li, D.; Zhang, Y.; Xu, Y.; Mater. Res. Bull. 2013, 48, 2268.
DOI:10.1016/j.materresbull.2013.02.016

24. Suh, J. Y.; Lopez, R.; Feldman, L. C.; Haglund, R. F.; J. Appl. Phys. 2004, 96, 1209.
DOI:10.1063/1.1762995

25. Kumar, R. T. R.; Karunagaran, B.; Mangalaraj, D.; Narayandass, S. A. K.; Manoravi, P.; Joseph M.; J. Mater. Sci. 2004, 39, 2869.
DOI: 10.1023/B:JMSC.0000021467.53474.e3

26. Klimov, V. A.; Timofeeva, I. O.; Khanin, S. D.; Shadrin, E. B.; Il'inskiĬ, A. V.; Silva-Andrade, F.; Semiconductors 2003, 37, 370.
DOI: 10.1134/1.1568452

27. Ilinski, A.; Silva-Andrade, F.; Shadrin, E.; Klimov, V.; J. Non-Cryst. Solids 2004, 338–340, 266.
DOI:10.1016/j.jnoncrysol.2004.02.083

28. Kang, L.; Gao, Y.; Zhang, Z.; Du, J.; Cao, C.; Chen, Z.; Luo, H.; J. Phys. Chem. C 2010, 114, 1901.
DOI: 10.1021/jp909009w

29. Beteille, F.; Livage, J.; J. Sol-Gel Sci. Techn. 1998, 13, 915.
DOI: 10.1023/A:1008679408509

30. Karaoglan-Bebek, G.; Hoque, M. N. F.; Holtz, M.; Fan, Z.; Bernussi, A. A.; Appl. Phys. Lett. 2014, 105, 201902.
DOI: 10.1063/1.4902056

.